Capacitive and Charge Transfer Effects of Single-Walled Carbon nanotubes in TiO_2 Electrodes

A. Ansón-Casaos, C. Rubio-Muñoz, J. Hernández-Ferrer, A. Santidrián, A.M. Benito, and W.K. Maser

ChemPhysChem 2019, 20, 838-847

Metallic and semiconducting carbon nanotube features observed in a hybrid titanium dioxide electrode

A. Ansón-Casaos,* C. Rubio-Muñoz, J. Hernández-Ferrer, A. Santidrian, A. M. Benito and W. K. Maser

Instituto de Carboquímica, ICB-CSIC, Miguel Luesma Castán 4, 50018 Zaragoza, Spain

Corresponding autor E-mail: alanson@icb.csic.es

Abstract

A commercial single-walled carbon nanotube (SWCNT) material is separated into various fractions containing different conformations. The liquid fractions show clear variations in their optical absorbance spectra, indicating differences in the metallic/semiconducting character and the diameter of the SWCNTs. However, all the thin solid films fabricated with the starting SWCNT sample and the fractions behave as semiconducting networks. The starting SWCNT sample and the fractions as well are used to prepare hybrid electrodes with titanium dioxide (5% SWCNT/TiO_2). Raman spectroscopy shows the transference of optoelectronic properties of the SWCNT fractions to SWCNT/TiO_2 electrodes. The electrochemical behavior of SWCNT/TiO_2 electrodes is studied by cyclic voltammetry. Voltammogram shape and faradaic peaks depend on the SWCNT fraction, showing a relationship between the SWCNT optical response and SWCNT/TiO_2 electrochemical properties. This work deepens into the transference of SWCNT nanoscale properties to macroscopic systems, which is a topic

of intense research for its fundamental interest and applications in electronics, energy devices, photocatalysis, and electroanalysis.

Keywords: carbon nanotube; semiconductor; optical spectroscopy; electronic properties; electrochemistry

1. Introduction

The properties of single-walled carbon nanotubes (SWCNTs) are mostly derived from their one-dimensional character, which produces confinement in the energy density of states. The cylindrical configuration of carbon atoms, commonly described through the Hamada indexes (*n,m*) control the electronic and vibrational response of individual SWCNTs. Therefore, SWCNTs show characteristic signals in their visible-near infrared absorption, photoluminescence and Raman spectra.[1-5]

In spite of the important progress in SWCNT synthesis, the currently available powder materials still consist of a mixture of many individual configurations. Several methods have been developed for the post-synthesis separation of SWCNTs, including density gradient ultracentrifugation,[6] gel chromatography,[7] and more recently, aqueous two-phase extraction.[8] In particular, gel chromatography methods were first described for HiPco® SWCNTs, and then extended to other SWCNT types.[9] One fraction of metallic species and a few fractions of mainly semiconducting species can be obtained by relatively simple experimental procedures at a laboratory scale.[10] In addition, highly specific separations have been described, including SWCNT enantiomer

isolation, although they require much complex time-consuming fractionation protocols.[11,12]

All the SWCNT separation methods require a previous stage of powder dispersion in a liquid, which ideally leads to stabilization and individualization. Since pristine SWCNTs are highly hydrophobic, dispersion in water has to be achieved using surfactants and ultrasonic treatments.[13] The resulting stable dispersions, either containing the pristine SWCNTs or after the chromatographic separation, can be processed by a wide range of deposition techniques including inkjet printing, roll-to-roll, dip-coating and spray-coating.[14-17] The as-prepared films, wires, circuits, coatings or interphases are ready for applications in electronics, sensors and energy devices, among others. Therefore, an interesting topic is whether the individual SWCNT electronic properties can be transferred to macroscopic film systems.

Metal oxide semiconductors are widely investigated for a great number of applications including solid state devices, electronics, solar cells and photocatalysis. In particular titanium dioxide (TiO_2) shows high photoactivity, chemical stability, abundance, low cost, biocompatibility and other relevant properties. Hibridization with carbon nanomaterials can be considered a way for modifying and improving TiO_2 performance.[18] Since synergistic effects in the composite materials are usually associated to processes taking place at interphase regions, it is expected that they will be enhanced using nanostructured materials, which show high surface areas and aspect ratios.

In the present work, pristine SWCNTs are separated into four fractions by gel chromatography at ambient conditions. One fraction mostly contains metallic SWCNTs and the others represent different distributions of semiconducting

SWCNTs. The predominant species in each fraction are identified by absorbance spectroscopy. The SWCNT fractions are utilized for the preparation of semi-transparent films and characterized by electrical conductivity measurements in the temperature range between 4 and 400 K. Then, the SWCNT dispersions are mixed with TiO_2 nanoparticles and deposited in the form of SWCNT/TiO_2 film electrodes. The transfer of SWCNT optical properties to the SWCNT/TiO_2 electrodes is shown by Raman spectroscopy. Electrochemical characterization by cyclic voltammetry show several faradaic features that can be intuitively assigned to redox processes on SWCNT/TiO_2 junctions. Moreover, the electrode double-layer capacitance and the faradaic features depend on the composition of the SWCNT fraction, demonstrating a relationship between the optical SWCNT properties and the electrochemical behaviour of the macroscopic hybrid network.

2. Experimental methods

2.1. Materials and equipment

Pristine HiPco® SWCNTs were purchased from NanoIntegris Technologies Inc., Boisbriand, Canada. Sodium dodecyl sulphate (SDS, 98%) was purchased from Sigma-Aldrich. Sodium deoxycholate (DOC, 99%, Across Organics) and Aeroxide® P25 TiO_2 were purchased from Fisher Scientific.

The alyl dextran gel Sephacryl S-200 (GE Healthcare) was utilized for the chromatographic separation. Standard 1mm glass slides and conductive silver paint (RS Components) were utilized for sheet resistance measurements. Fluorinated tin oxide (FTO, 80 nm on 1mm glass slides, 25x10 mm^2, R ~ 100 Ω/sq.) substrates were provided by Solems SA, Palaiseau, France.

Ultrasound treatments were performed with a 400 W UP400S probe by Hielscher, Germany, working at 0.5 cycles and 60% amplitude. Centrifugation was performed in an Optima L-100XP ultracentrifuge by Beckman Coulter, provided with a SW55Ti 3671 rotor. The 475 Premium spray gun by Sagola, Vitoria, Spain, was utilized for film deposition.

Absorption spectra were performed in Shimadzu UV-2401 PC and FTIR Vertex 70 Bruker spectrometers, using cuvettes of 1 cm optical path. Four probe electrical conductivity measurements were performed in a Physical Property Measurement System, model 6000 PPMS controller.

Raman spectra were measured using a HORIBA Jobin Yvon spectrometer HR 800UV. The measuring parameters were set as follows: laser wavelength = 532 nm (green) or 785 nm (red), hole = 500 μm, grating = 1800 lines/mm, exposition = 5 s, accumulation = 5 acquisitions, objective = x50. The incident power was around 1 mW.

Electrochemical measurements were carried out in a three electrode configuration using the Autolab PGSTAT 302N. The reference electrode was Ag/AgCl, 3M NaCl (E° = 0.210 V), and the counter electrode was a graphite rod. Cyclic voltammetry was performed at a scan rate of 20 mV/s.

2.2. Chromatographic separation

In a typical experiment, 10 mg of SWCNT powder was mixed with 10 mL of 0.5% SDS and sonicated for 1 h in an ice bath. The dispersions were centrifuged at 200,000xg (40,500 rpm) for 90 min at 20°C. The supernatant was carefully decanted and the sediment discarded. The resulting liquid suspension contains highly purified well-dispersed SWCNTs.[17,19,20]

A vertical plastic syringe of 50 mL ($Ø_i$ = 29 mm) with a steel needle was utilized as the chromatographic column. The separation was performed by gravity at ambient conditions of temperature and pressure. The chromatography gel was inserted in the column up to a height of 12 mm, and packed by washing with water and 0.5% SDS. The liquid flow was set at approximately 1mL·min^{-1} by means of a cotton plug at the syringe exit.

Immediately after gel packing, 8 mL of the purified SWCNT dispersion was carefully added at the top of the gel column, and a first reddish fraction was eluted. Three additional fractions were eluted by the subsequent addition of 8 mL of 1% SDS, 2% SDS and 1% DOC. The starting purified dispersion and the four eluted fractions are hereafter called 0-SWCNT and i-SWCNT, where i is the fraction number.

2.3. Optical absorption spectra

Absorbance spectra were measured in the ultraviolet-visible-near infrared (UV-Vis-NIR) region from 300 to 1350 nm. The technique provides semi-quantitative information about the SWCNT conformations present in the liquid suspension. In addition, the SWCNT concentration (c) after centrifugation can be determined if the relationship of absorbance (A) vs. c is known at a given wavelength λ. The calibration was performed by measuring the absorbance for several dispersions of the pristine SWCNT material. According to the Beer-Lambert law: $A = \varepsilon \cdot L \cdot c$, where L = 1 cm is the optical path of the quartz cuvette, an extinction coefficient ε = 22.7 mL·mg^{-1}·cm^{-1} was determined at λ = 850 nm, and it was considered to be approximately constant for all the SWCNT dispersions.

2.4. Specimens for electrical resistance measurements

Resistance measurements were performed on semi-transparent films made from the purified and separated SWCNT dispersions. Perfectly clean square glass substrates ($10 \cdot 10 \cdot 1$ mm^3) were used as supports. The preparation of SWCNT thin films was performed by spray-coating the aqueous dispersions on the substrates at 125°C. Approximately 1 mL of SWCNT dispersion at 0.02 mg·mL^{-1} was painted on each substrate. The films were immersed in deionized water overnight to remove the surfactant. Two silver electrodes were painted on opposite sides of the square specimen, where electrodes were connected for the measurement.

2.5. Preparation of SWCNT/TiO_2 electrodes

In a typical experiment, 1 mL of a 2 mg·mL^{-1} suspension of TiO_2 in absolute ethanol was prepared by bath sonication for 30 min. Subsequently, a suitable volume of the SWCNT aqueous dispersion was added and homogenised in the ultrasounds bath. The SWCNT amount was the 5.5 mass% of the TiO_2. The SWCNT/TiO_2 hybrid material was deposited on approximately 1 cm^2 of the FTO substrate by spray-coating. Dry films were washed by immersion in deionized water for 24 h for the removal of the surfactant residue. Finally, the films were sintered at 450°C for 1 h under nitrogen atmosphere.

3. Results and discussion

3.1. Optical absorption study

Figure 1 shows UV-Vis-NIR spectra of the starting SWCNT suspension and the four fractions separated in the chromatography column. The fractions present different colours, more specifically red, brownish, green and blue, which reflect

their different optical response. In the first fraction, most of the SWCNTs are metallic (M-SWCNT), confirming the successful separation between M-SWCNTs and semiconducting species (S-SWCNT) in 0.5% SDS. The S-SWCNTs remain in the chromatography gel due to their stronger interaction, while M-SWCNTs are eluted. It has been shown that SWCNT adsorption on the gel is endothermic, and substantial differences exist between adsorption enthalpies of M- and S-SWCNTs.[21]

The first reddish fraction shows increased absorbance bands in the range of 400-650 nm, which are associated to electronic transitions between the first van Hove singularities in M-SWCNTs (M_{11} transitions). Three bands are observed in the M_{11} region, related to various conformations of M-SWCNTs. Various M-SWCNT types were tentatively identified by their *(n,m)* indexes (Table S1), and associated to their respective diameters, according to the literature.[1,22,23] The diameters are represented against their respective absorption peak wavelengths in the bottom panel of Figure 1.

After the 1-SWCNT fraction, which mainly shows the absorbance bands of M-SWCNTs, the S-SWCNTs are eluted, starting by nanotubes with the largest diameters. The 2-SWCNT fraction contains various S-SWCNT conformations (Table S2), and a contribution of M-SWCNTs that is detected at absorbances around 510 and 555 nm. The most intense absorbance bands appear in the region of S_{11} transitions. Nanotubes with large diameters in the range of 14-19 nm are detected through their S_{22} transitions. The 3-SWCNT fraction contains many types of S-SWCNTs but only a residual presence of the M-SWCNT bands at 510 and 555 nm. Intense absorption bands are detected in the regions of both the S_{11} and S_{22} transitions. Several nanotube families with small diameters in the range

of 7-9 nm are detected through their S_{11} transitions, indicating that the average nanotube diameter decreases with respect to the previous 2-SWCNT fraction. Finally, the blueish 4-SWCNT fraction is eluted, including all the nanotubes that remained in the column after the previous elution. A residual presence of M-SWCNTs is detected around 460 and 510 nm. The most prominent bands are associated to S-SWCNTs with small diameters (6-11 nm), while the number of conformational families with large diameters strongly decrease (Figure 1).

3.2. Electrical characterization

The electronic transport properties of SWCNT thin films, which were prepared by spray coating from the starting 0-SWCNT dispersion and the chromatographic fractions as well, were studied through measurements of DC resistance (R) in the temperature range of 4 to 400 K (Figure 2). It is known that R values are influenced by ambient conditions such as moisture and the filling gas in the measurement chamber.[24,25] The present measurements were performed under vacuum, after waiting for at least 2 h at room temperature, during which the film resistance increased until stabilization.

For all the i-SWCNT films, R increases as temperature decreases, particularly below 70 K. Independently of the individual SWCNT conformations, all the SWCNT networks show a semiconductor behaviour, even though the resistance variation with temperature is much slower than in classical semiconductors such as germanium.[26] The shape of the R vs. T curve is analogous for all the measured films, in agreement with the fact that they are of nearly identical thicknesses.[26] The steep increase in R at $T < 70$ K can be fitted to tunnelling

transport models, while the slow variation at T > 70 K is associated to thermal effects.[26]

In the whole studied temperature range, the lowest R (the highest conductivity) is found for the film prepared from the starting 0-SWCNT dispersion, and not for any of the fractions. The R values increase following the order of elution in the chromatographic column: 0 < 1 < 2 < 3. The film that was prepared with the 4-SWCNT fraction led to a very high R, which could not be measured in the utilized experimental setup. The metallic characteristics of individual nanotubes from the 1-SWCNT fraction are not reflected in the behaviour of the film network. This fact might be due to a decrease in the length/diameter aspect ratio of the SWCNTs or SWCNT bundles during the chromatographic separation, which would cause an increase in the number of inter-nanotube contacts needed to create conducting paths in the network. It is evident that the electrical behaviour of the SWCNT thin film is not determined by individual nanotubes, but by contact resistances between them, in agreement with recent literature works.[27,28] Here, the electrical characterization of pure SWCNT films has to be taken in mind for the interpretation of the SWCNT/TiO_2 electrochemical response.

3.3. Raman spectroscopy

The optoelectronic properties of the SWCNT/TiO_2 electrodes were studied by Raman spectroscopy with two laser excitation wavelengths at 532 and 785 nm (green and red). The Raman modes of anatase phase TiO_2, which is the main component of commercial Aeroxide® P25, were observed at 140, 190, 390, 520 and 640 cm^{-1} (not shown), in good agreement with the literature.[29]

For the present study, the most interesting features are the SWCNT bands, particularly the radial breathing modes (RBMs) in the region of 175-300 cm^{-1} and the tangential modes (TMs) at around 1600 cm^{-1} (Figure 3). Raman spectroscopy is a resonant technique, and the signal intensity strongly depends on the laser excitation wavelength. Small or even residual amounts of SWCNT species near resonance conditions produce much stronger intensities than larger amounts of out-of-resonance SWCNTs. Therefore, the present measurements are only qualitative from the viewpoint of individual (*n,m*) SWCNTs. For instance, small amounts of a M-SWCNT conformation can be detected in samples that mostly contain S-SWCNTs, and vice versa.

With the green laser, prominent RBMs for the 0-SWCNT/TiO_2 film are observed at 184, 230, 239, 247, 263 and 271 cm^{-1}. Clear differences are detected in the SWCNT/TiO_2 electrodes prepared with the SWCNT fractions from the chromatography column. Some of the features change their relative intensities, while the bands at 260 and 271 cm^{-1} are maintained in all the fractions. The 1- and 2-SWCNT/TiO_2 films keep the metallic M_{11} bands in the region of 225-260 cm^{-1}, while the intensity decreases in the 3- and 4- SWCNT/TiO_2. The 2-SWCNT/TiO_2 particularly looks like the starting 0-SWCNT/TiO_2, and this fact will be later associated with the electrochemical results. The band at around 184 cm^{-1} decreases while that at 295 cm^{-1} increases in the spectra of 3- and 4-SWCNT/TiO_2 films, showing that progressive changes take place during the chromatographic extraction. Most specifically, large diameter S-SWCNTs disappear while small diameter S-SWCNTs appear in the last fractions, in agreement with absorbance results in the liquids.

The TMs under the green laser undergo a clear evolution with the progress of the chromatographic separation (Figure 3.b). The starting sample shows a prominent G^- band at 1550 cm^{-1}, which can be associated to the presence of metallic SWCNT conformations.[30] The prominent G^- band appears in the 1- and 2-SWCNT/TiO_2 samples, but it is progressively lost for 3- and 4-SWCNT/TiO_2. Therefore, the M-SWCNT conformations in resonance under the green laser were mostly captured in the first and second fractions of the chromatographic extraction.

Under the red laser, the RBMs of the 0-SWCNT/TiO_2 sample appear at 209, 219, 229, 236, 248, 261 and 269 cm^{-1} (Figure 3.c). The bands at 209 and 219 cm^{-1}, which are associated to large diameter S-SWCNTs, nearly disappear in the 3- and 4-SWCNT fractions. The TM profiles are nearly identical for all the samples (Figure 3.d), since the M-SWCNT conformations are far from resonance under the laser excitation at 785 nm.

In summary, Raman spectroscopy on the SWCNT/TiO_2 electrodes confirms that the liquid phase separation of SWCNTs is reflected in the optoelectronic properties of the solid composite. In the following, it will be proved that changes in the conformational composition of the SWCNT samples also affect the electrochemical characteristics of the composite SWCNT/TiO_2 electrodes.

3.4. Electrochemical analysis

The chromatographic separation of SWCNT dispersions into different conformational compositions largely modifies the electrochemical response of SWCNT/TiO_2 electrodes, which is here analysed by cyclic voltammetry in an alkaline medium (Figure 4). Figure 4.a shows the response of a pure TiO_2 film on

the FTO substrate. The current density increases exponentially at the most negative potentials (E < -1.2 V vs. Ag/AgCl), as the TiO_2 conduction band is filled with electrons. The exponential shape is usually associated to the presence of electronic states inside the bandgap, near to the lowest conduction band level, which are originated at the edge defects of TiO_2 nanoparticles.[31]

The voltammogram of the 0-SWCNT/TiO_2 electrode, containing 5% of the starting SWCNT material, is totally different from the blank TiO_2. Various anodic and cathodic peaks appear, particularly around E = -0.8 V. In pure SWCNT electrodes, incipient faradaic peaks have been previously associated to the SWCNT reduction process, whose redox potentials have been evaluated and depend on the SWCNT (*n,m*) conformation.[32,33] In hybrid SWCNT/TiO_2 electrodes, the peaks seem to be amplified by a charge transfer from TiO_2 close to the SWCNT reduction potential.[34] Since the potentials depend on the (*n,m*) indexes, it has to be expected that voltammogram peaks will change for the different SWCNT chromatographic fractions. In fact, the prominent peaks of the 0-SWCNT/TiO_2 electrode clearly show an effect of fractionation.

The voltammogram of the 1-SWCNT/TiO_2 electrode, which mainly contains M-SWCNT conformations, is quite rectangular-shaped and reaches high current values, indicating an increased double-layer capacitance. Synergistic improvements in the double-layer capacitance have been reported in carbon xerogel/TiO_2,[35] multi-walled carbon nanotube/TiO_2,[36,37] and graphene/TiO_2 electrodes.[38,39] The increase in capacitance has been typically associated to surface area and electrical conductivity given by the nanostructured carbon materials. However, it is demonstrated here that the suitable electronic characteristics or energy levels of the SWCNT fillers are also decisive for the

resulting electrode behaviour, since not all the SWCNT fractions lead to identical results. Moreover, it has to be remembered here that all the i-SWCNT networks show analogous electrical transport characteristics (Section 3.2), so the observed behaviour of SWCNT/TiO_2 electrodes has to be related to SWCNT individual properties rather than to the conducting network.

Together with the double-layer capacitance improvement, the prominent anodic/cathodic peaks that are observed in the 0-SWCNT/TiO_2 nearly disappear in the 1-SWCNT/TiO_2. Therefore, the M-SWCNT conformations in the first fraction provide charge accumulation surfaces but not charge transfer interfaces in the studied potential window. On the contrary, the 2-SWCNT/TiO_2 electrode shows many peaks, which are reminiscent of the 0-SWCNT/TiO_2 electrode. The SWCNT conformations that provide charge transfer centres for TiO_2 were mostly separated in the second fraction of the chromatographic column. Besides, this hypothesis agrees with the similar Raman spectra of the 0-SWCNT and 2-SWCNT/TiO_2 electrodes.According to optical absorbance and Raman results, certain large diameter S-SWCNT conformations might play a key role in the faradaic charge transfer from TiO_2.

The 3- and 4-SWCNT/TiO_2 electrodes show some of the initial faradaic charge transfer peaks; however, all of them are relatively weak. In addition, both the cathodic and anodic current densities, and thus the double layer capacitances, are lower than in the 1-SWCNT/TiO_2. Overall, it is shown that the capacitance and the peaks in the voltammograms of SWCNT/TiO_2 electrodes depend on the conformational composition of the SWCNT dispersion utilized for their preparation.

4. Conclusions

In the present work, it is confirmed that SWCNT liquid dispersions of different conformational compositions can be obtained by chromatographic fractionation at ambient conditions. Independently of the M-SWCNT concentration, all the SWCNT solid films behave as semiconducting networks. However, hybrid 5% SWCNT/TiO_2 electrodes prepared with the SWCNT fractions keep their respective optical properties, as measured by Raman spectroscopy, and show different electrochemical response. A high concentration of M-MWCNTs (1-SWCNT/TiO_2) leads to an increased double-layer capacitance with no faradaic features. In the measured potential window (-1.4 to 0.0 V vs. Ag/AgCl), faradaic peaks appear to be associated to certain large diameter S-SWCNT species (1-SWCNT/TiO_2), which provide the most suitable energetics for charge transfer from TiO_2. The other S-SWCNTs (3- and 4-SWCNT/TiO_2) lead to comparatively low double-layer capacitance and weak faradaic peaks. This work reveals a relationship between optical properties of SWCNTs and the electrochemical response of SWCNT/TiO_2 hybrid electrodes, and suggests new ideas to transfer nanoscale properties into macroscopic systems.

Acknowledgements

Special thanks are directed to the Service of Physical Measurements at the University of Zaragoza (Dr. A. Arauzo) and the Analysis Service of Instituto de Carboquímica (Ms. A. Díaz). This work has been funded by the Spanish Ministry of Science and the European Regional Development Fund (ENE 2016-79282-C5-1-R), the Government of Aragon (T03-17R), and the European Commission (H2020-MSCA-ITN-2014-ETN 642742 “Enabling Excellence”).

References

[1] M. S. Strano, S. K. Doom, E. H. Haroz, C. Kittrell, R. H. Hauge and R. E. Smalley, *Nano Lett.* **2003**, *3*, 1091-1096.

[2] R. B. Weisman and S. M. Bachilo, *Nano Lett.* **2003**, *3*, 1235-1238.

[3] S. Lebedkin, F. Henrich, T. Skipa and M. M. Kappes, *J. Phys. Chem. B* **2003**, *107*, 1949-1956.

[4] V. Barone, J. E. Peralta and G. E. Scuseria, *Nano Lett.* **2005**, *5*, 1830-1833.

[5] P. T. Araujo, P. B. C. Pesce, M. S. Dresselhaus, K. Sato, R. Saito and A. Jorio, *Physica E* **2010**, *42*, 1251-1261.

[6] M. S. Arnold, S. I. Stupp and M. C. Hersam, *Nano Lett.* **2005**, *5*, 713-718.

[7] H. Liu, D. Nishide, T. Tanaka and H. Kataura, *Nature Commun.* **2011**, *2*, 309.

[8] J. A. Fagan, C. Y. Khripin, C. A. Silvera Batista, J. R. Simpson, E. H. Haroz, A. R. Hight Walker and M. Zheng, *Adv. Mater.* **2014**, *26*, 2800-2804.

[9] J. Zhang, H. Gui, B. Liu, J. Liu and C. Zhou, *Nano Res.* **2013**, *6*, 906-920.

[10] A. J. Blanch, J. S. Quinton and J. G. Shapter, *Carbon* **2013**, *60*, 471-480.

[11] H. Liu, T. Tanaka, Y. Urabe and H. Kataura, *Nano Lett.* **2013**, *13*, 1996-2003.

[12] T. Tanaka, Y. Urabe, T. Hirakawa and H. Kataura, *Anal. Chem.* **2015**, *87*, 9467-9472.

[13] V. C. Moore, M. S. Strano, E. H. Haroz, R. H. Hauge and R. E. Smalley, *Nano Lett.* **2003**, *3*, 1379-1382.

[14] Y. Yu, H. Wada, J. Inoue, S. Imaizumi, Y. Kounosu, K. Tsuboi, H. Matsumoto, M. Ashizawa, T. Mori, M. Minagawa and A. Tanioka, *Appl. Phys. Express* **2011**, *4*, 115101.

[15] B. Dan, G. C. Irvin and M. Pasquali, *ACS Nano* **2009**, *3*, 835-843.

[16] F. Mirri, A. W. K. Ma, T. T. Hsu, N. Behabtu, S. L. Eichmann, C. C. Young, D. E. Tsentalovich and M. Pasquali, *ACS Nano* **2012**, *6*, 9737-9744.

[17] A. Ansón-Casaos, R. Mis-Fernández, C. M. López-Alled, E. Almendro-López, J. Hernández-Ferrer, J. M. González-Domínguez and M. T. Martínez, *Chem. Eng. Sci.* **2015**, *138*, 566-574.

[18] A. Ansón-Casaos, M. J. Sampaio, C. Jarauta-Córdoba, M. T. Martínez, C. G. Silva, J. L. Faria, A. M. T. Silva, *Chem. Eng. J.* **2015**, *277*, 11-20.

[19] A. J. Blanch, C. E. Lenehan, J. S. Quinton, *Carbon* **2011**, *49*, 5213-5228.

[20] A. Ansón-Casaos, J. M. González-Domínguez, I. Lafragüeta, J. A. Carrodeguas and M. T. Martínez, *Carbon* **2014**, *66*, 105-118.

[21] A. Hirano, T. Tanaka and H. Kataura, *ACS Nano* **2012**, *6*, 10195-10205.

[22] C. Fantini, A. Jorio, M. Souza, M. S. Strano, M. S. Dresselhaus, M. A. Pimenta, *Phys. Rev. Lett.* **2004**, *93*, 147406.

[23] H. Telg, J. Maultzsch, S. Reich, F. Hennrich, C. Thompsen, *Phys. Rev. Lett.* **2004**, *93*, 177401.

[24] I. Sayago, E. Terrado, M. Aleixandre, M. C. Horrillo, M. J. Fernández, J. Lozano, E. Lafuente, W. K. Maser, A. M. Benito, M. T. Martínez, J. Gutiérrez, E. Muñoz, *Sens. Actuat. B: Chem.* **2007**, 122, 75-80.

[25] A. Roch, M. Greifzu, E. R. Talens, L. Stepien, T. Roch, J. Hege, N. V. Nong, T. Schmiel, I. Dani, C. Leyens, O. Jost, A. Leson, *Carbon* **2015**, *95*, 347-353.

[26] M. E. Itkis, A. Pekker, X. Tian, E. Bekyarova, R. C. Haddon, *Acc. Chem. Res.* **2015**, *48*, 2270-2279.

[27] H. Jeong, J. Park, *J. Phys. Chem. C* **2015**, *119*, 9665-9668.

[28] A. Stern, S. Azoubel, E. Sachyani, G. I. Livshits, D. Rotem, S. Magdassi, D. Porath, *J. Phys. Chem. C* **2018**, *122*, 14872-14876.

[29] A. Turkovic, M. Ivanda, A. Drasner, V. Vranesa, M. Persin, *Thin Solid Films* **1991**, *198*, 199-205.

[30] N. Bendiab, R. Almairac, M. Paillet, J. L. Sauvajol, *Chem. Phys. Lett.* **2003**, *372*, 210-215.

[31] T. Berger, D. Monllor-Satoca, M. Jankulovska, T. Lana-Villarreal, R. Gómez, ChemPhysChem 2012, 13, 2824-2875.

[32] S. A. Hodge, M. K. Bayazit, H. H. Tay, M. S. P. Shaffer, *Nature Commun.* **2013**, *4*, 1989.

[33] Y. Hirana, G. Juhasz, Y. Miyauchi, S. Mouri, K. Matsuda, N. Nakashima, *Sci. Rep.* **2013**, *3*, 2959.

[34] A. Ansón-Casaos, J. Hernández-Ferrer, C. Rubio-Muñoz, A. Santidrian, M. T. Martinez, A. M. Benito, W. K. Maser, *ChemElectroChem* **2017**, *4*, 2300-2307.

[35] A. Elmouwahidi, E. Bailón-García, J. Castelo-Quibén, A. F. Pérez-Cárdenas, F. J. Maldonado-Hódar, F. Carrasco-Marín, *J. Mater. Chem. A* **2018**, *6*, 633-644.

[36] C. Chien, S. S. Deora, P. Chang, D. Li, J. G. Lu, *IEEE T. Nanotechnol.* **2011**, *10*, 706-709.

[37] B. Zhang, R. Shi, Y. Zhang, C. Pan, *Prog. Nat. Sci. Mater.* **2013**, *23*, 164-169.

[38] P. Yadav, K. Pandey, P. Bhatt, B. Tripathi, M. K. Pandey, M. Kumar, *Mater. Sci. Eng. B* **2016**, *206*, 22-29.

[39] P. Nagaraju, A. Alsalme, A. Alswieleh, R. Jayavel, *J. Electroanal. Chem.* **2018**, *808*, 90-100.

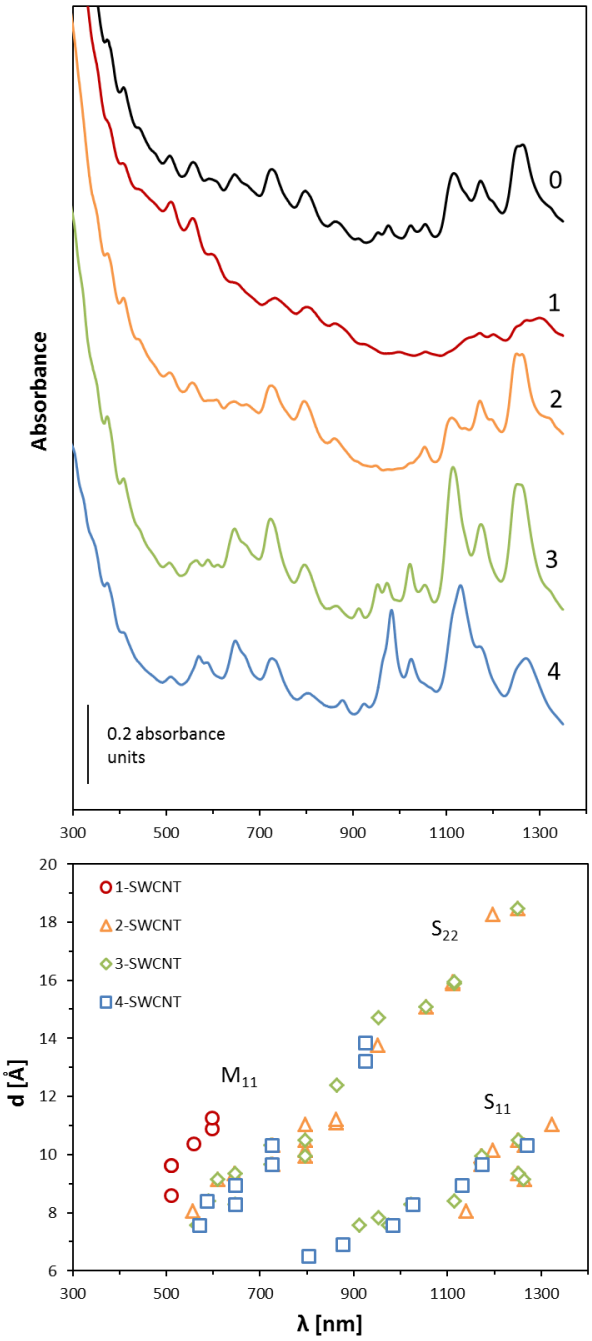

Figure 1. Top) absorbance spectra of the diluted pristine SWCNT aqueous dispersion and the four fractions extracted from the chromatography column; bottom) tentative assignation of prominent peaks to SWCNT diameters.

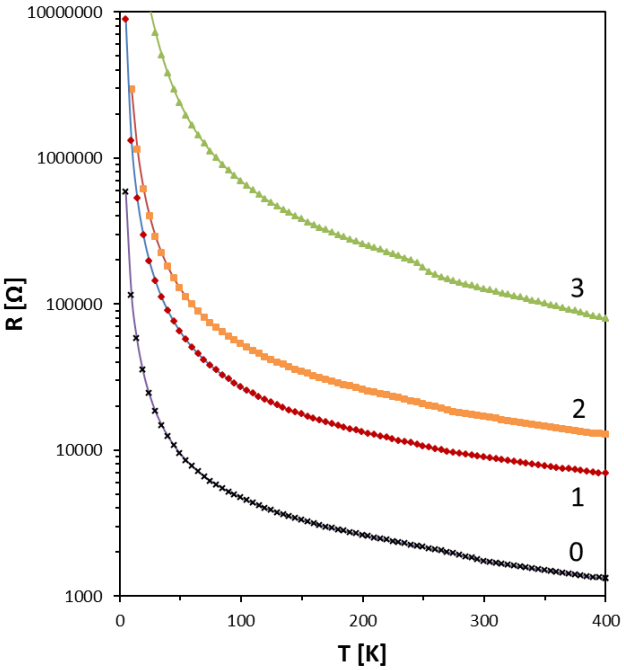

Figure 2. Electrical resistance measurements on semi-transparent films of the pristine 0-SWCNTs and three fractions extracted from the chromatography column.

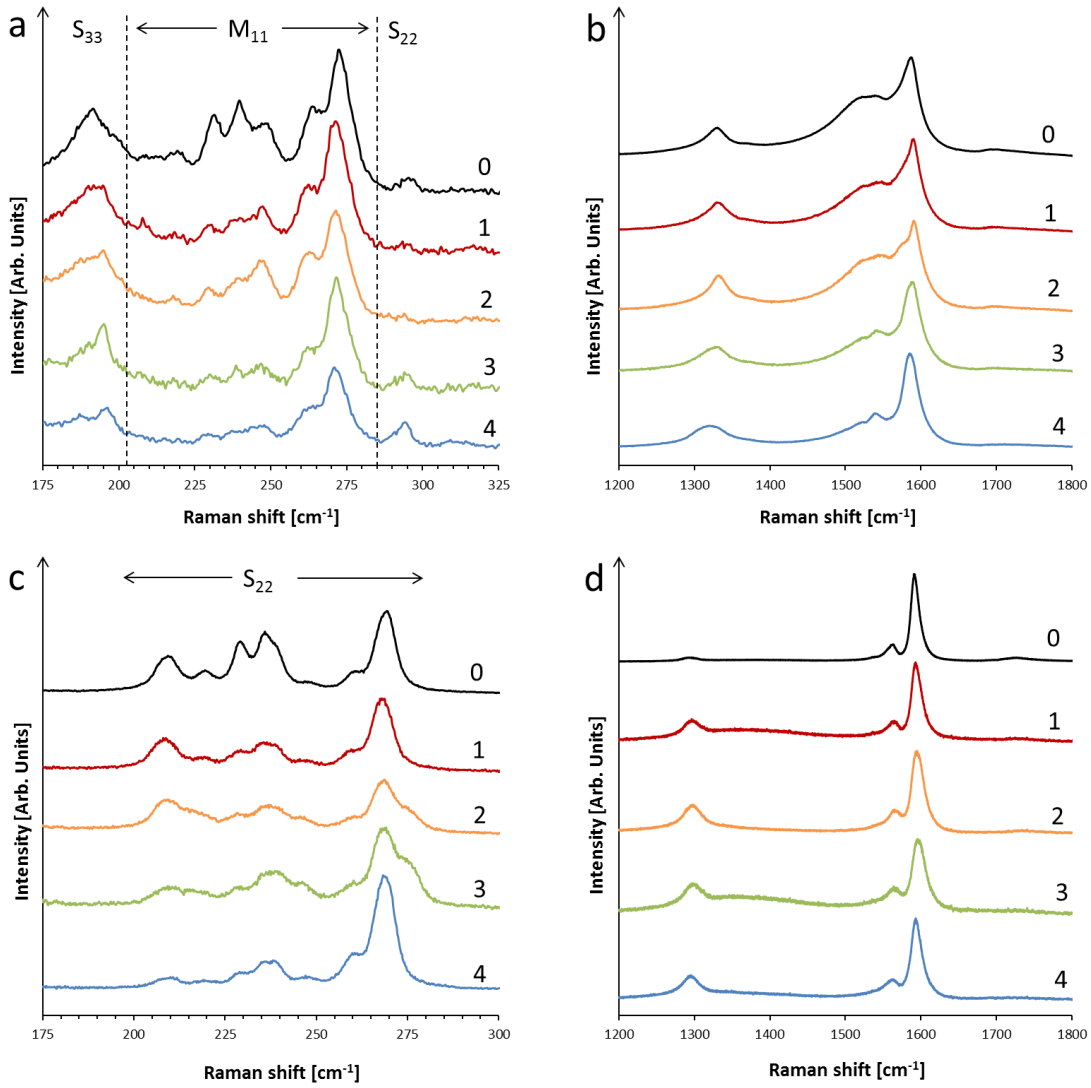

Figure 3. Raman spectra of i-SWCNT/TiO_2 films obtained with: a, b) 532 nm green laser, and c, d) 785 nm red laser excitations, in the regions of: a, c) RBMs, and b, d) TMs.

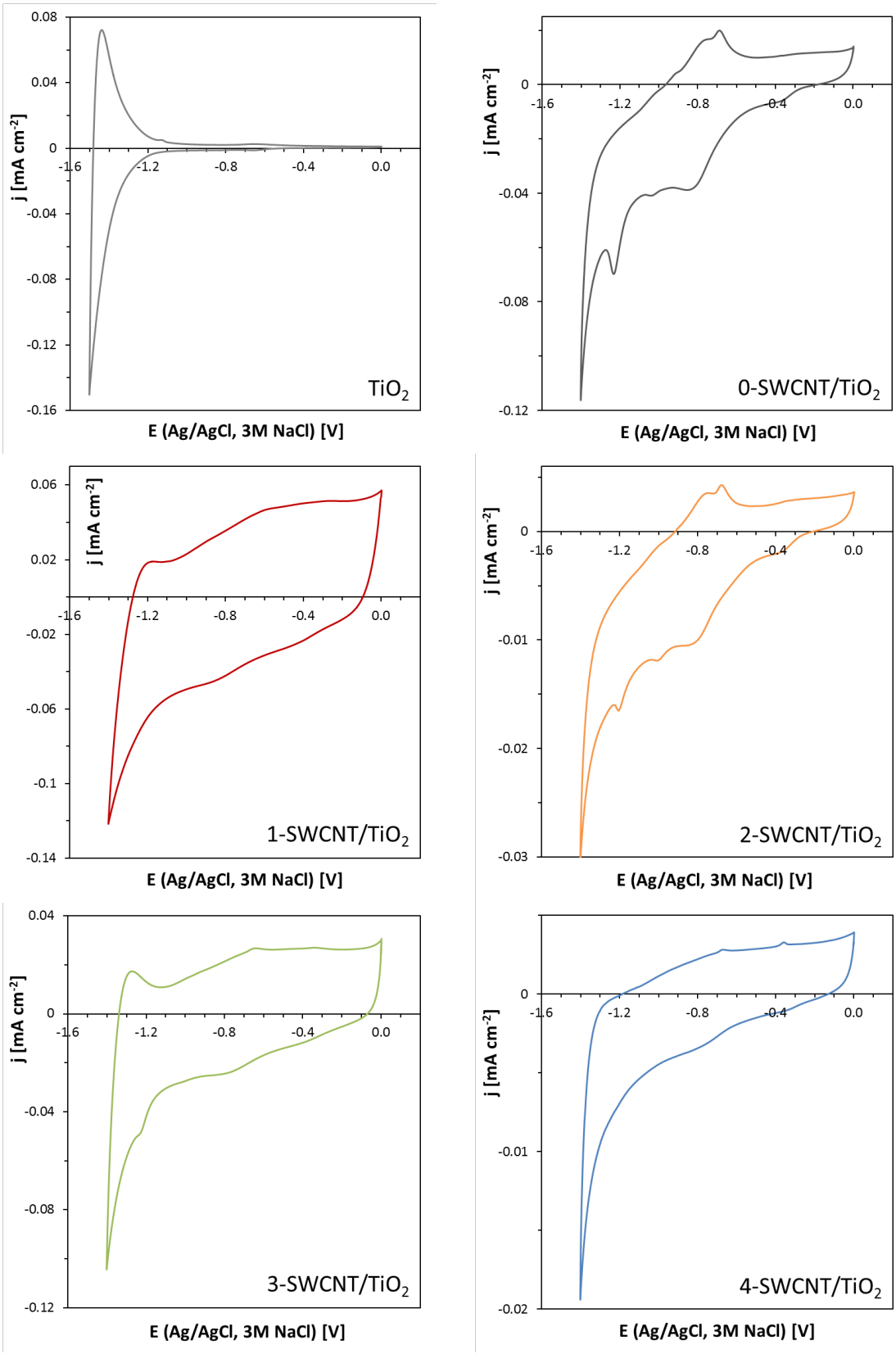

Figure 4. Cyclic voltammetry study of the blank TiO_2 and i-SWCNT/TiO_2 electrodes.